THE JOURNAL OF CLINICAL PSYCHIATRY
THE OFFICIAL JOURNAL OF THE AMERICAN SOCIETY OF CLINICAL PSYCHOPHARMACOLOGY

# Supplementary Material

**Article Title:** Altered Topological Patterns of Brain Networks in Remitted Late-Onset Depression:A Resting-State fMRI Study

**Author(s):** Zan Wang, MD; Yonggui Yuan, MD, PhD; Feng Bai, MD; Jiayong You, MD; and Zhijun Zhang, MD, PhD

**DOI Number:** dx.doi.org/10.4088/JCP.14m09344

## List of Supplementary Material for the article

1. eAppendix 1 Supplemental METHOD
2. eTable 1 Cortical and Subcortical Regions of Interest Defined in the Study
3. eTable 2 Raw Scores of Neuropsychological Tests
4. eFigure 1 A Flowchart for The Construction of Functional Brain Networks
5. eFigure 2 Scatter Plots of Topological Properties (Both Global and Regional Metrics) and Neuropsychological Scores in rLOD Patients

## Disclaimer

This Supplementary Material has been provided by the author(s) as an enhancement to the published article. It has been approved by peer review; however, it has undergone neither editing nor formatting by in-house editorial staff. The material is presented in the manner supplied by the author.

**Altered Topological Patterns of Brain Networks in Remitted Late-onset Depression: A Resting-State fMRI Study**

**eAppendix 1**

## Supplemental METHOD

### Participants

All rLOD patients met the following inclusion criteria: (1) they had previously met the major depression disorder in DSM-IV criteria and remitted for more than 6 months before the enrollment; (2) the age of first depressive onset was over 60 years; (3) Hamilton Depression Rating Scale (HDRS) scores were lower than 7, and Mini-Mental State Examination (MMSE) scores were higher than 24; (4) duration of illness must be less than 5 years and a medication-free period for all patients was longer than 3 months prior to the assessment; (5) absence of other major psychiatric disorder, including hidden abuse or dependence of psychoactive substances; (6) absence of primary neurological illness, including dementia or stroke; (7) absence of medical illness impairing cognitive function; (8) no history of electroconvulsive therapy; (9) no gross structural abnormalities on T1-weight images, and no major white matter changes such as infarction or other vascular lesions on T2-weight MRI.

### Imaging Acquisition

All subjects were scanned using a General Electric 1.5 Tesla scanner (General Electric Medical Systems, USA) with a homogeneous birdcage head coil. Axial R-fMRI (no cognitive tasks were performed, eyes were closed, and ears were occluded) datasets were obtained in seven minutes and six seconds with a single-shot gradient-recalled echo-planar imaging (GRE-EPI) sequence: TR =

3000 ms; TE = 40 ms; FA = 90°; acquisition matrix = 64 × 64; FOV = 240 mm × 240 mm; thickness = 4.0 mm; gap = 0mm and 3.75 mm × 3.75 mm in-plane resolution.

**Imaging Preprocessing**

Imaging preprocessing was carried out using the Statistical Parametric Mapping (SPM8, http://www.fil.ion.ucl.ac.uk/spm) and Data Processing Assistant for Resting-State fMRI (DPARSF, http://www.restfmri.net/forum /dparsf). The first ten volumes were discarded for scanner stabilization and participants' adaption to the circumstances. The remaining images were corrected for timing differences and motion effects. Participants with head motion more than 3mm maximum displacement in any direction of *x*, *y* and *z* or 3 degree of any angular motion were excluded. Subsequently, the resulting images were spatially normalized into the stereotaxic space using an optimum, 12-parameter affine transformation and nonlinear deformation, and then resampled to 3 × 3 × 3 $mm^3$ voxels. Further preprocessing included linear detrend and temporal band-pass filtering (0.01-0.1Hz), which were used to reduce the effects of low-frequency drift and high frequency physiological respiratory and cardiac noise. Finally, the nuisance signals involving six head motion parameters, global mean signal, cerebrospinal fluid signal, and white matter signal were regressed out from the data.

**Network Construction**

To construct the brain functional network, the images of each brain were first parcellated into 90 regions of interest (ROIs, Supplementary eTable 1) using the automated anatomically labeling atlas, which has been broadly used in several previous brain network studies[1-3]. Then the representative time series of each ROI were obtained by simply averaging the fMRI time series over all voxels in this region. Pearson correlation coefficients between each pair of 90 ROIs were subsequently

calculated, thus generating a 90 × 90 correlation matrix for each subject. To avoid complicated statistical descriptions in the following network analysis, our graph theoretical analysis is confined to a simple undirected and unweighted binary matrix (Supplementary eFigure 1). Each absolute correlation matrix was thresholded into a binary matrix with a fixed sparsity level, *S* (defined as the number of edges in a graph divided by the maximum possible number of edges of the graph). Setting a sparsity threshold ensured that all the resultant networks had the same number of edges[3, 4]. As there is no gold standard for a single threshold, we thresholded each absolute correlation matrix repeatedly over a wide range of sparsity levels ($10\% \leq S \leq 34\%$) at an interval of 0.01, and calculated the parameters of the resulting graphs with different thresholds.

**Network Analysis**

*Small-world Parameters*

The small-world parameters of a network (clustering coefficient $C_p$, and characteristic path length $L_p$) were originally proposed by Watts and Strogatz[5]. Briefly, the $C_p$ of a network is the average of the clustering coefficients over all nodes, where the clustering coefficient $C_i$ of a node is defined as the ratio of the number of existing connections among the node's neighbors and all their possible connections. $C_p$ quantifies the local interconnectivity of a network. $L_p$ of a network is the shortest path length (numbers of edges) required to transfer from one node to another averaged over all pairs of nodes. $L_p$ indicates the overall routing efficiency of a network. To estimate the small-world properties, we scaled $C_p$ and $L_p$ derived from the brain networks with the mean $C_p^{rand}$ and $L_p^{rand}$ of 100 random networks (i.e., $\gamma = C_p / C_p^{rand}$ and $\lambda = L_p / L_p^{rand}$ ) that preserved the same number of nodes, edges and degree distributions as the real networks[6]. A small-world network should fulfill the conditions of $\gamma > 1$ and $\lambda \approx 1$[5], and therefore, the small-worldness scalar $\sigma = \gamma / \lambda$ will be more than

1[7].

*Network Efficiency*

The global efficiency measures the ability of parallel information transmission over the network[8]. For a network *G* with *N* nodes and *K* edges, the global efficiency of *G* can be computed as:

$$E_{glob}(G) = \frac{1}{N(N\text{-}1)} \sum_{i \neq j \in G} \frac{1}{L_{ij}},$$

where $L_{ij}$ is the shortest path length between node *i* and node *j* in *G*.

The local efficiency measures the fault tolerance of the network, indicating the capability of information exchange for each subgraph when the index node is eliminated. The local efficiency of *G* is measured as:

$$E_{loc}(G) = \frac{1}{N} \sum_{i \in G} E_{glob}(G_i),$$

where $G_i$ denotes the subgraph composed of the nearest neighbors of node *i*.

*Regional Nodal Characteristics*

To evaluate the roles of brain regions (or nodes) in brain networks, we computed the regional efficiency $E_{nodal}(i)$[4]. Nodal efficiency measures the information propagation ability of a node with the rest of nodes in the network. The nodal efficiency of node *i* is computed as:

$$E_{nodal}(i) = \frac{1}{N(N\text{-}1)} \sum_{i \neq j \in G} \frac{1}{L_{ij}},$$

where $L_{ij}$ is the shortest path length between node *i* and node *j* in *G*.

**Statistical Analysis**

*Behavioral Data*

To increase statistical power by reducing random variability, a composite score analysis was utilized, as previously introduced[9]. First, the raw scores from each test for each subject were

transformed to *z* scores with reference to the means and standard deviations of each test for all subjects. Second, all neuropsychological tests were grouped into four cognitive domains and the related composite scores were calculated by averaging the *z* scores of the individual tests according to the following divisions: Episodic Memory (two test, including AVLT-DR and CFT-DR), Visuospatial Skills (two tests, including CFT and CDT), Processing Speed (two tests, including SDMT and TMT-A) and Executive Function (two tests, including DST and TMT-B).

*Network Metrics*

Between-group differences in topological attributes (both global and regional measures) were investigated by nonparametric permutation tests[10]. First, we calculated the between-group difference in the mean value of each network metric. To test the null hypothesis that the observed group differences could occur by chance, we randomly reallocated each subject to one of the two groups and recomputed the mean differences between the two randomized groups. The randomization procedure was repeated 10,000 times, and a randomized null distribution based on between-group differences in each metric was created. Then the 95% percentile point of the distribution was used as the critical value for two-tail test of the null hypothesis. This permutation test procedure was repeated at the sparsity of $10\% \leq S \leq 34\%$. In addition, the same permutation procedure was used to compare the AUC of network measures between groups. Of note, before the permutation tests, multiple linear regression analyses were applied to remove the confounding effects of age, gender and years of education for each network metric.

**Supplemental REFERENCES**

1. Sanz-Arigita EJ, Schoonheim MM, Damoiseaux JS, et al. Loss of 'small-world' networks in Alzheimer's disease: graph analysis of FMRI resting-state functional connectivity. *PloS One* 2010;5(11):e13788.

2. Yao Z, Zhang Y, Lin L, et al. Abnormal cortical networks in mild cognitive impairment and Alzheimer's disease. *PLoS Comput Biol* 2010;6(11):e1001006.

3. Zhang J, Wang J, Wu Q, et al. Disrupted brain connectivity networks in drug-naive, first-episode major depressive disorder. *Biol Psychiatry* 2011;70(4):334-342.

4. Achard S, Bullmore E. Efficiency and cost of economical brain functional networks. *PLoS Comput Biol* 2007;3(2):e17.

5. Watts DJ, Strogatz SH. Collective dynamics of 'small-world' networks. *Nature* 1998;393(6684):440-442.

6. Maslov S, Sneppen K. Specificity and stability in topology of protein networks. *Science* 2002;296(5569):910-913.

7. Humphries MD, Gurney K, Prescott TJ. The brainstem reticular formation is a small-world, not scale-free, network. *Proc Biol Sci* 2006;273(1585):503-511.

8. Latora V, Marchiori M. Efficient behavior of small-world networks. *Phys Rev Lett* 2001;87(19):198701.

9. Sexton CE, McDermott L, Kalu UG, et al. Exploring the pattern and neural correlates of neuropsychological impairment in late-life depression. *Psychol Med* 2012;42(6):1195-1202.

10. Bullmore ET, Suckling J, Overmeyer S, Rabe-Hesketh S, Taylor E, Brammer MJ. Global, voxel, and cluster tests, by theory and permutation, for a difference between two groups of structural MR images of the brain. *IEEE Trans Med Imaging* 1999;18(1):32-42.

**Supplementary eTable 1 Cortical and Subcortical Regions of Interest Defined in the Study**

| Index | Regions | Abbreviation | Index | Regions | Abbreviation |
|---|---|---|---|---|---|
| (1,2) | Precentral gyrus | PreCG | (47,48) | Lingual gyrus | LING |
| (3,4) | Superior frontal gyrus, dorsolatera | SFGdor | (49,50) | Superior occipital gyrus | SOG |
| (5,6) | Superior frontal gyrus, orbital part | ORBsup | (51,52) | Middle occipital gyrus | MOG |
| (7,8) | Middle frontal gyrus | MFG | (53,54) | Inferior occipital gyrus | IOG |
| (9,10) | Middle frontal gyrus, orbital part | ORBmid | (55,56) | Fusiform gyrus | FFG |
| (11,12) | Inferior frontal gyrus, opercular pa | IFGoperc | (57,58) | Postcentral gyrus | PoCG |
| (13,14) | Inferior frontal gyrus, triangular pa | IFGtriang | (59,60) | Superior parietal gyrus | SPG |
| (15,16) | Inferior frontal gyrus, orbital part | ORBinf | (61,62) | Inferior parietal, but supramarginal and angular gy | IPL |
| (17,18) | Rolandic operculum | ROL | (63,64) | Supramarginal gyrus | SMG |
| (19,20) | Supplementary motor area | SMA | (65,66) | Angular gyrus | ANG |
| (21,22) | Olfactory cortex | OLF | (67,68) | Precuneus | PCUN |
| (23,24) | Superior frontal gyrus, medial | SFGmed | (69,70) | Paracentral lobule | PCL |
| (25,26) | Superior frontal gyrus, medial orbi | ORBsupmed | (71,72) | Caudate nucleus | CAU |
| (27,28) | Gyrus rectus | REC | (73,74) | Lenticular nucleus, putamen | PUT |
| (29,30) | Insula | INS | (75,76) | Lenticular nucleus, pallidum | PAL |
| (31,32) | Anterior cingulate and paracingulate gyri | ACG | (77,78) | Thalamus | THA |
| (33,34) | Median cingulate and paracingulate gyri | DCG | (79,80) | Heschl gyrus | HES |
| (35,36) | Posterior cingulate gyrus | PCG | (81,82) | Superior temporal gyrus | STG |
| (37,38) | Hippocampus | HIP | (83,84) | Temporal pole: superior temporal gyrus | TPOsup |
| (39,40) | Parahippocampal gyrus | PHG | (85,86) | Middle temporal gyrus | MTG |
| (41,42) | Amygdala | AMYG | (87,88) | Temporal pole: middle temporal gyrus | TPOmid |
| (43,44) | Calcarine fissure and surrounding cortex | CAL | (89,90) | Inferior temporal gyrus | ITG |
| (45,46) | Cuneus | CUN | | | |

Note: The regions are listed according to a prior template obtained from an AAL atlas.

**Supplementary eTable 2 Raw Scores of Neuropsychological Tests**

| **Measures** | **rLOD** (n=33) | **HC** (n=31) | ***P* values** |
|---|---|---|---|
| Episodic memory | | | |
| AVLT-DR | 6.55 ± 2.37 | 8.23 ± 1.75 | 0.001 [a] |
| CFT-DR | 15.47 ± 7.64 | 16.79 ± 6.55 | 0.520 [a] |
| Executive function | | | |
| DST | 12.48 ± 2.51 | 13.16 ± 2.08 | 0.118 [a] |
| TMT-B (second) | 209.42 ± 119.91 | 132.10 ± 37.26 | 0.000 [a] |
| Processing speed | | | |
| SDMT | 27.36 ± 14.18 | 35.97 ± 9.85 | 0.000 [a] |
| TMT-A (second) | 117.30 ± 84.62 | 67.97 ± 24.77 | 0.000 [a] |
| Visuospatial skills | | | |
| CFT | 30.74 ± 8.36 | 34.48 ± 1.75 | 0.003 [a] |
| CDT | 8.27 ± 2.14 | 8.97 ± 1.02 | 0.221 [a] |

Data are presented as mean (M) ± stand deviation (SD).

Abbreviations: rLOD, remitted late-onset depression; HC, healthy controls; AVLT-DR, auditory verbal learning test-delayed recall; CFT-DR, rey-osterrieth complex figure test-delayed recall; DST, digit span test; TMT, trail-making test; SDMT, symbol digit modalities test; CDT, clock drawing test.

Note: [a] Analysis of covariance (ANCOVA)

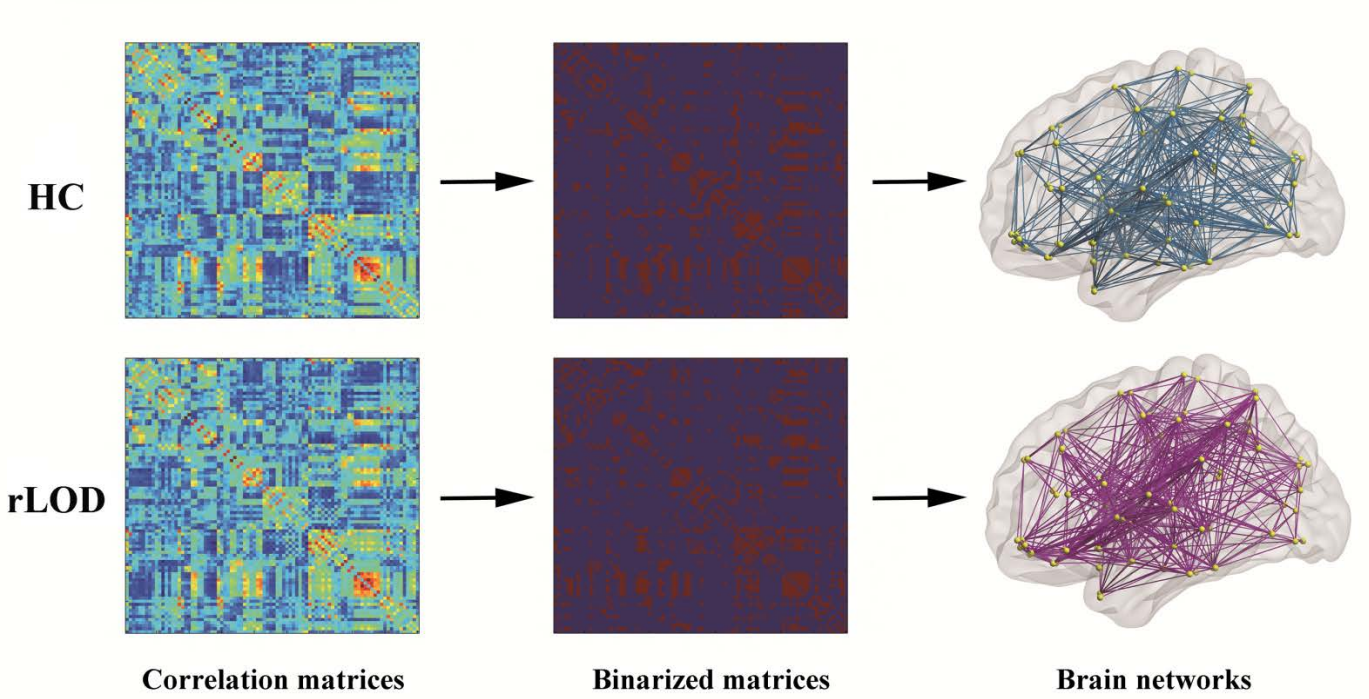


**Supplementary eFigure 1 A Flowchart for The Construction of Functional Brain Networks.** Left, both in rLOD and HC groups, a correlation matrix was obtained for each subject by calculating inter-regional Pearson correlation coefficient of mean time series among 90 regions; Middle, these correlation matrices were further converted into binarized matrices by applying a thresholding procedure; Right, the obtained binary matrices could be finally represented as networks or graphs that were composed of brain nodes and edges. rLOD, remitted late-onset depression; HC, healthy controls.

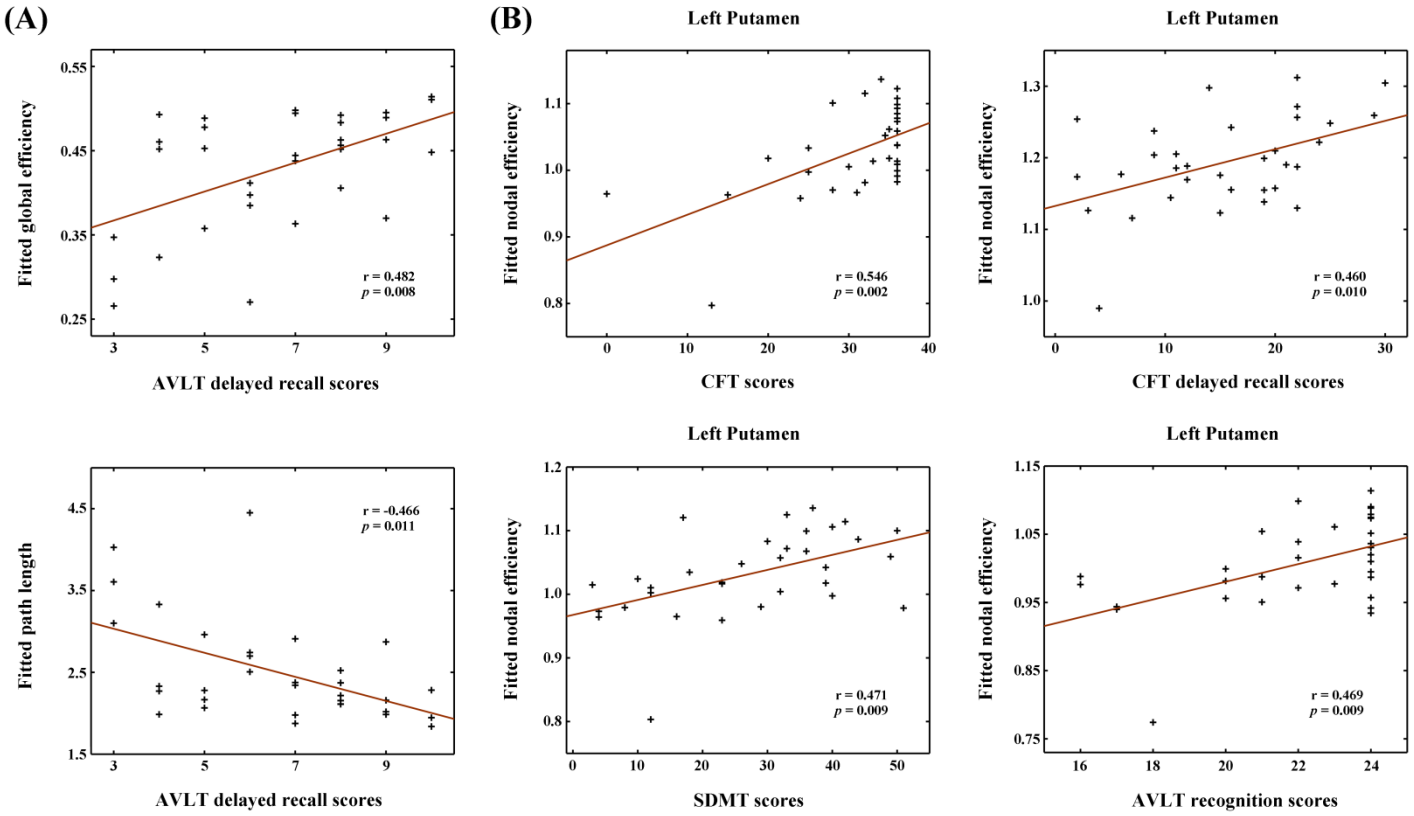


**Supplementary eFigure 2 Scatter Plots of Topological Properties (Both Global and Regional Metrics) and Neuropsychological Scores in rLOD Patients.** (**A**) The correlations between AVLT-DR scores and $L_p$ and $E_{glob}$. (**B**) The correlations between nodal efficiency of left putamen and CFT, CFT-DR, SDMT and AVLT-recognition scores. rLOD, remitted late-onset depression; AVLT-DR, auditory verbal learning test-delayed recall; CFT, rey-osterrieth complex figure test; SDMT, symbol digit modalities test.